(Received 29 April 2024, Accepted 14 June 2024, Scheduled 29 June 2024)

Design of Double-Layer Circular Polarization Multiplex Focusing Metasurface Lens

Honggang Hao, Zhonglyu Cai*, Bao Li, and Pan Tang

School of Optoelectronic Engineering, Chongqing University of Posts and Telecommunications, Chongqing, China

ABSTRACT: Addressing the problem of Pancharatnam-Berry (PB) phase metasurface mutual coupling and single functionality under orthogonal circularly polarized wave incidence, a circularly polarized multiplexing focusing metasurface lens with polarization conversion functionality operating at 24 GHz is proposed using the method of jointly modulating PB phase and resonance phase. The metasurface unit is composed of two layers of dielectric plates covered with metal patterns on both sides separated by air. By varying the parameter sizes of each joint of the windmill-shaped metal pattern, the resonance phase of the unit can be independently controlled in the x-polarization and y-polarization directions, achieving a phase coverage close to 320° while maintaining a transmission magnitude greater than 0.8. By rotating the metal pattern, the size of the PB phase can be freely controlled. Adjusting the parameters of the metal pattern, the unit has a phase difference of 180° in the x- and y-polarization directions, achieving polarization conversion of circularly polarized waves, with its polarization conversion ratio (PCR) approaching 100% near the operating frequency band. Simulation and test results show that under left-handed and right-handed circularly polarized wave incidence, the metasurface lens achieves single-point focusing effects at different positions, with focusing efficiencies of 45.6% and 45.9%, and focal spot sizes of -3 dB of 8.8 mm and 8.4 mm, respectively. This work is expected to be applied in fields such as K-band satellite communication, wireless power transmission, and 24 GHz automotive millimeter-wave radar.

1. INTRODUCTION

Circularly polarized waves are electromagnetic waves in which the projection of the endpoint of the electric field vector onto a plane perpendicular to the direction of propagation forms a circle. Based on the direction of variation of the electric field vector, they can be classified as left-handed circularly polarized (LHCP) waves and right-handed circularly polarized waves (RHCP). Circularly polarized waves have unchanged electric field strength during propagation, and the direction of the electric field changes regularly with time and space, effectively reducing the multipath effect and signal attenuation during propagation. In engineering, circularly polarized waves can be received using linearly polarized antennas in any orientation, offering significant advantages in communication scenarios where the relative positions of the transmitter and receiver are constantly changing. In space communication, circularly polarized waves can overcome polarization rotation caused by Faraday rotation, enabling effective propagation through the Earth's ionosphere. Therefore, circularly polarized waves are widely utilized in fields such as satellite communication [1, 2], radar [3, 4], and space remote sensing [5].

Metasurfaces are artificial planar electromagnetic structures capable of flexibly manipulating the amplitude and phase characteristics of electromagnetic waves. They possess advantages of high integration and simple manufacturing, exhibiting significant advantages in controlling electromagnetic wavefronts, and are widely applied in fields such as optical imaging [6], wireless communication [7, 8], and medical sensing [9, 10]. Metasurfaces also serve as excellent media for achieving electromagnetic wave focusing. By simply manipulating the phase distribution of the metasurface, electromagnetic waves can be focused at the desired positions. There are mainly two types of metasurface phase control technologies: resonance phase control [11, 12] and Pancharatnam-Berry (PB) phase control [13, 14]. For the focusing of linearly polarized waves, the resonance phase principle is typically employed to control their transmission phases, thereby focusing the outgoing waves at the target positions. In 2018, Chu et al. proposed a metasurface lens with a coaxial annular aperture structure based on resonance phase, achieving high-resolution near-field focusing of millimeter waves [15]. In 2019, Zhang et al. proposed a polarization-sensitive near-field reflective focusing metasurface based on resonance phase and anisotropy, realizing independent control of the incident wave's x-polarization and y-polarization components [16]. The designed metasurface achieved different focusing functions under the incidence of x-polarized and y-polarized waves at 10 GHz. For circularly polarized waves, PB phase principle is typically used to control their transmission phases. In 2016, Guo et al. proposed a single-layer ultra-thin circularly polarized focusing metasurface lens, which can convert LHCP waves at 15 GHz into RHCP waves and focus the transmitted waves in the near field [17]. Currently, most reported metasurfaces can only achieve single-function focusing. Although some researchers have proposed linear polarization multiplexing metasurfaces based on the anisotropy of metasurface structures to achieve

* Corresponding author: Zhonglyu Cai (s210401001@stu.cqupt.edu.cn).

two different focusing functions under x- and y-polarized wave incidence [21, 25]. However, there is little research on metasurfaces for circularly polarized wave multiplexing focusing. Phase modulation uses PB phase as a common method for metasurfaces to control the wavefront of circularly polarized waves. When two orthogonal circularly polarized waves enter the metasurface, conjugate and opposite PB phases are obtained. This restricts the repeated use of circularly polarized waves to some extent.

In this paper, we propose a structure combining resonance phase and PB phase [18, 19], which consists of circular resonators surrounding windmill-shaped metallic patches. By varying the parameters of the unit structure, independent control of the resonance phase in the x- and y-polarization directions is achieved, with a phase coverage of 320 degrees under the condition of transmission amplitude exceeding 0.8. By changing the rotation angle of the unit structure, the PB phase of the unit is controlled, and by combining PB phase and resonance phase, decoupling of orthogonal circularly polarized PB phases is achieved, enabling different focusing functions under the incidence of LHCP and RHCP waves. The simulation analysis results are consistent with the physical measurement ones.

2. DESIGN OF METASURFACE UNIT

The Pancharatnam-Berry phase was first proposed by Berry in 1984 [20]. In microwave systems, when the polarization state of an electromagnetic wave changes from an initial state and returns to the initial polarization state, an additional phase is generated. The magnitude of this phase difference equals half the solid angle enclosed by the path of variation in the Poincaré sphere. For planar structures, the PB phase is represented by a change of $\pm 2\theta$ in the phase of the cross-polarization component when the element structure is rotated θ degrees perpendicular to the plane. The propagation of electromagnetic waves in metasurfaces can be described using Jones matrices. The propagation of circularly polarized waves in space can be represented as:

$$\begin{cases} \vec{E}_R = \left[\begin{array}{cc} E_{0x}e^{j(\omega t-kz+\varphi_x)} & jE_{0y}e^{j(\omega t-kz+\varphi_y)} \end{array} \right]^T \\ \vec{E}_L = \left[\begin{array}{cc} jE_{0x}e^{j(\omega t-kz+\varphi_x)} & E_{0y}e^{j(\omega t-kz+\varphi_y)} \end{array} \right]^T \end{cases} \quad (1)$$

where ω is the angular frequency; k is the wave number; E_x and E_y are the electric field components of the electromagnetic wave in the x- and y-polarization directions; and φ_x and φ_y are the initial phases. The transmission Jones matrix for a metasurface unit rotating θ around the z-axis can be represented as:

$$\tilde{T}(\theta) = MTM^{-1} = \left(\begin{array}{cc} \cos\theta & \sin\theta \\ -\sin\theta & \cos\theta \end{array} \right) \left(\begin{array}{cc} t_{xx} & t_{xy} \\ t_{yx} & t_{yy} \end{array} \right) \left(\begin{array}{cc} \cos\theta & \sin\theta \\ -\sin\theta & \cos\theta \end{array} \right)^{-1} \quad (2)$$

Without considering time and space variations, the transmitted electromagnetic field can be expressed as [21]:

$$\left(\begin{array}{c} E_+^t \\ E_-^t \end{array} \right) = \left(\begin{array}{c} \frac{1}{2}\left[t_{xx}+t_{yy}+j\left(t_{xy}-t_{yx}\right)\right] \\ \frac{1}{2}e^{-j2\theta}\left[t_{xx}-t_{yy}+j\left(t_{xy}+t_{yx}\right)\right] \end{array} \right.$$
$$\left. \begin{array}{c} \frac{1}{2}e^{j2\theta}\left[t_{xx}-t_{yy}-j\left(t_{xy}+t_{yx}\right)\right] \\ \frac{1}{2}\left[t_{xx}+t_{yy}-j\left(t_{xy}-t_{yx}\right)\right] \end{array} \right) \left(\begin{array}{c} E_+^{in} \\ E_-^{in} \end{array} \right) \quad (3)$$

From Equation (3), it can be seen that when the incident wave is circularly polarized, the phase of the transmitted wave's co-polarization component remains unchanged, while the cross-polarization component introduces a phase φ with a magnitude of $\pm 2\theta$, where $\varphi = 2\theta$ for LHCP waves and $\varphi = -2\theta$ for RHCP waves. According to the above principles, it is possible to control the phase of the cross-polarization component of the incident wave by adjusting the angle of the unit structure rotation. However, for LHCP and RHCP, this phase is conjugate. To achieve the reuse of circularly polarized waves, it is necessary to introduce additional phases for decoupling. Let $\varphi_-(x_i, y_j)$ and $\varphi_+(x_i, y_j)$ represent two different phase distributions required to achieve the desired function under the incidence of LHCP and RHCP waves, respectively. The metasurface transmission Jones matrix $T(x_i, y_j)$ needs to satisfy the following conditions simultaneously:

$$\begin{cases} T\left(x_i, y_j\right) \cdot L = \exp\left[j\varphi_-\left(x_i, y_j\right)\right] \cdot R \\ T\left(x_i, y_j\right) \cdot R = \exp\left[j\varphi_+\left(x_i, y_j\right)\right] \cdot L \end{cases} \quad (4)$$

The two-dimensional Jones vectors of LHCP and RHCP waves can be represented as: $L = [1j]^T$ and $R = [1\ -\ j]^T$, so Equation (4) can be expressed as:

$$T\left(x_i, y_j\right) = \left[\begin{array}{cc} \frac{1}{2}[e^{j\varphi_-(x_i,y_j)} + e^{j\varphi_+(x_i,y_j)}] & \frac{1}{2}[e^{j\varphi_+(x_i,y_j)} - e^{j\varphi_-(x_i,y_j)}] \\ \frac{1}{2}[e^{j\varphi_+(x_i,y_j)} - e^{j\varphi_-(x_i,y_j)}] & -\frac{1}{2}[e^{j\varphi_+(x_i,y_j)} + e^{j\varphi_+(x_i,y_j)}] \end{array} \right] \quad (5)$$

According to the symmetry and unitarity of the matrix, $T(x_i, y_j)$ can be orthogonally transformed into:

$$T\left(x_i, y_j\right) = B\Lambda B^{-1} \quad (6)$$

where B is a skew-symmetric matrix, and Λ is a diagonal matrix. For metasurface unit with isotropy, the diagonal matrix Λ represents the resonant phases introduced by the metasurface element along two orthogonal polarization directions, $\varphi_x(x_i, y_j)$ and $\varphi_y(x_i, y_j)$, where the skew-symmetric matrix B represents the rotation angle $\theta(x_i, y_j)$ of the metasurface unit at that position. By combining Equations (5) and (6), we can obtain the relationships between the resonance phases $\varphi_x(x_i, y_j)$ and $\varphi_y(x_i, y_j)$, the unit rotation angle $\theta\left(x_i, y_j\right)$, and the desired phases $\varphi_-(x_i, y_j)$ and $\varphi_+(x_i, y_j)$, as shown below:

$$\varphi_x\left(x_i, y_j\right) = \left[\varphi_-\left(x_i, y_j\right) + \varphi_+\left(x_i, y_j\right)\right]/2 \quad (7)$$
$$\varphi_y\left(x_i, y_j\right) = \left[\varphi_-\left(x_i, y_j\right) + \varphi_+\left(x_i, y_j\right)\right]/2 - \pi \quad (8)$$
$$\theta\left(x_i, y_j\right) = \left[\varphi_-\left(x_i, y_j\right) - \varphi_+\left(x_i, y_j\right)\right]/4 \quad (9)$$

Therefore, when the unit PB phase and resonance phase satisfy Equations (7)–(9), the unit can exhibit different phase responses under LHCP and RHCP wave incidence. This demonstrates that by introducing resonance phase modulation, it is possible to decouple the PB phases of LHCP and RHCP, thus enabling the construction of two independent circular polarization channels in the same metasurface, providing a theoretical basis for

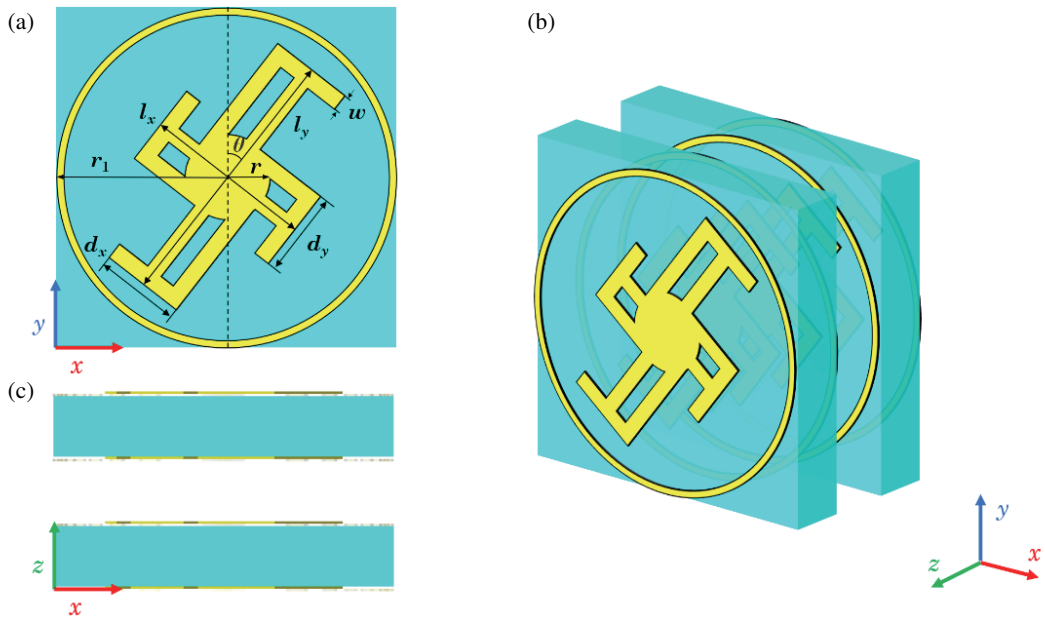

FIGURE 1. The schematic of the metasurface unit structure: (a) Front view of the unit structure. (b) Side view of the unit structure. (c) Shows the overall structure.

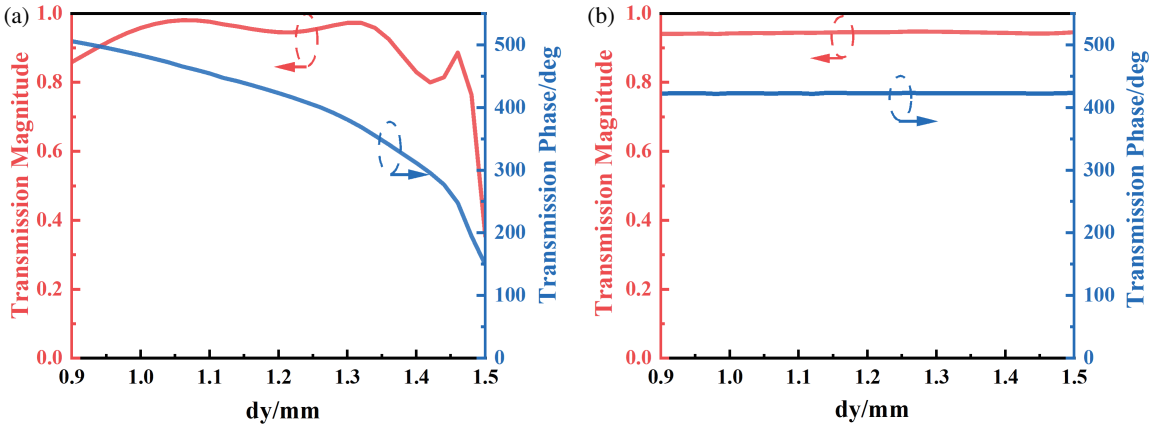

FIGURE 2. The relationship between the transmission amplitude and phase of the unit and the parameters under the incident x-polarized wave at 24 GHz. (a) Parameters lx and dy as variables; (b) Parameters ly and dx as variables.

the design of circular polarization-reusing transmissive focusing metasurfaces.

The proposed circularly polarized reconfigurable transmissive metasurface unit structure is shown in Fig. 1. The unit has a period of $P = 4.2$ mm, consisting of one layer of air, two layers of dielectric substrate, and four layers of metal. The material of the dielectric substrate is F4B, with a relative dielectric constant $\varepsilon_r = 2.65$ and a loss tangent $\delta = 0.004$. The thickness of the dielectric substrate and air layer is $h = 1$ mm. The metal layer consists of a rotatable windmill-type metal structure with a peripheral circular metal resonator. The material is copper with a thickness of $d = 0.035$ mm, and the rotation angle is θ. The radius of the circular metal resonator is $r_1 = 2$ mm with a thickness of 0.1 mm, and the circular patch radius at the center of the metal structure is $r = 0.5$ mm. The width of the multiple metal strips extending from the circular patch is fixed at $w = 0.2$ mm, while their lengths are varied and denoted by lx, ly, dx, and dy.

In order to verify whether the designed unit can flexibly control the resonant phase $\varphi_x(x_i, y_j)$ and $\varphi_y(x_i, y_j)$ in the x- and y-polarization directions, we model and simulate the unit in the electromagnetic simulation software CST. Under the incidence of x-polarized waves at 24 GHz, the rotation angle θ was 0, with fixed parameters $lx = 2dy$, $ly = 2dx = 1.2$ mm. When the parameters $lx/2$ and dy gradually changed from 0.9 mm to 1.5 mm, the transmission amplitude and phase of the unit are shown in Fig. 2(a). As lx and dy increase, the transmission amplitude of the unit changes, and the transmission phase in the

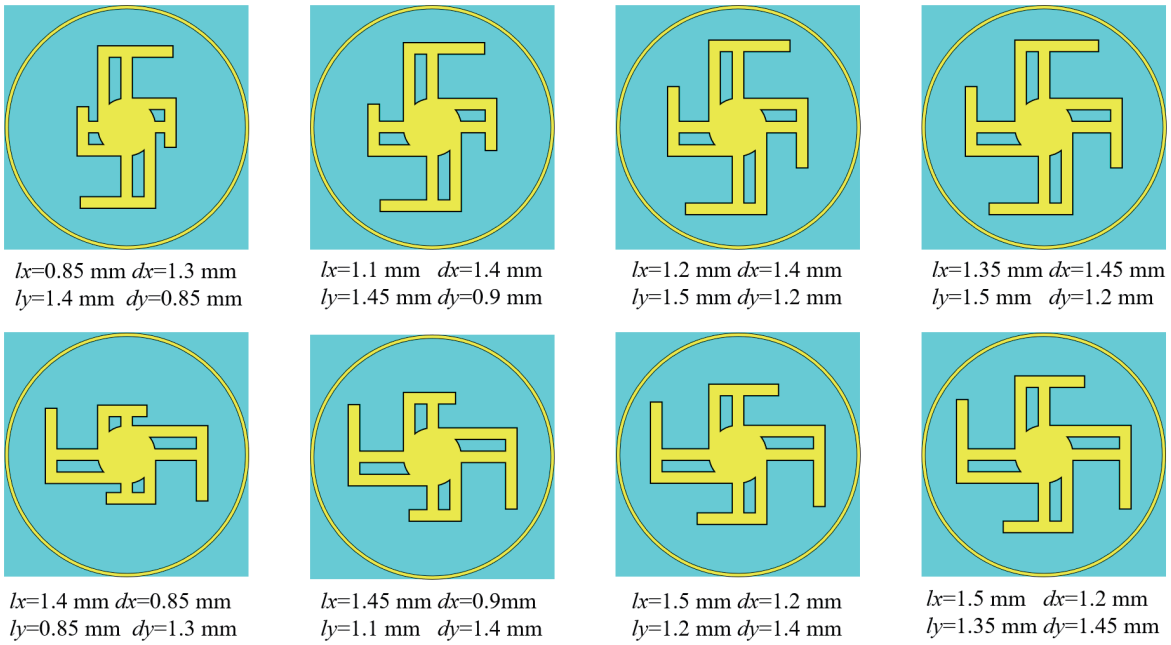

FIGURE 3. Selected 8 metasurface units.

x-polarization direction also gradually increases. At 24 GHz, within the range where the transmission amplitude of the unit is greater than 0.8, the phase shift range can reach 320°. This proves that flexible control of the transmission phase can be achieved by changing the size of the parameters. Similarly, with fixed parameters $lx = 2dy = 1.2$ mm and $ly = 2dx$, when $ly/2$ and dx gradually change from 0.9 mm to 1.5 mm, the transmission amplitude and phase of the unit are shown in Fig. 2(b). It can be observed that the transmission amplitude of the unit is all greater than 0.9, but changing the parameters ly and dx has almost no effect on the transmission amplitude and phase of the unit in the x-polarization direction. This proves that changes in parameters in the x- or y-polarization direction do not affect the transmission amplitude and phase in the y- or x-direction. The above results demonstrate that with the change of parameters, the metasurface unit can independently control the resonant phase of x- and y-polarizations of the metasurface while maintaining high transmission amplitude and achieve a wide range of phase shifts.

Based on the simulation results, using a phase difference of 45° as the phase gradient, the transmission phase of the discrete unit is obtained, thereby obtaining the structure of 8 different parameter metasurfaces, as shown in Fig. 3.

The electromagnetic simulation software CST was used to model and simulate the 8 units shown in Fig. 3. The transmission coefficients and phases of the 8 units under x- and y-polarization incidence can be obtained. Figs. 4(a) and (b) show the transmission amplitude and phase of the unit under x-polarized wave incidence, while Fig. 4(c) and Fig. 4(d) show the transmission amplitude and phase of the unit under y-polarized wave incidence. It can be observed that when the 24 GHz linearly polarized wave is incident, the transmission amplitudes of the 8 units are all greater than 0.8; the phase difference between adjacent units is 45°; the phase difference between x- and y-polarization directions of the same unit is 180°; and the above 8 units can achieve 360° full coverage of transmission phase in both x- and y-polarization directions.

When the phase difference between the x- and y-polarization directions of the unit is 180°, the incident left-handed (right-handed) circularly polarized wave can be converted into right-handed (left-handed) circularly polarized wave. To verify the polarization conversion performance of the unit, taking unit 1 as an example, assuming that the unit rotates counterclockwise around the z-axis with the geometric center as θ, where θ is the variable, under the incidence of LHCP waves, the amplitudes and phases of co-polarization and cross-polarization of the unit are shown in Fig. 5.

From Figs. 5(a) and (b), it can be observed that in the vicinity of the 24 GHz frequency band, when LHCP waves are incident, the co-polarization transmission amplitude of the unit is all less than 0.05, and with the change of θ, the co-polarization transmission phase hardly changes. The above results indicate that there is almost no LHCP component in the outgoing electromagnetic waves. From Fig. 5(c) and Fig. 5(d), it can be seen that the cross-polarization transmission amplitude of the unit near the 24 GHz frequency band is greater than 0.8. The phase difference of the cross-polarization transmission of units with a geometric rotation angle difference of θ is 2θ. This indicates that almost all of the LHCP waves entering the unit are converted into RHCP waves. The transmission phase of the outgoing wave satisfies the PB phase principle, proving that cross-polarization conversion occurs after circularly polarized incident waves enter the metasurface. The polarization conversion performance can be measured using the Polarization Conver-

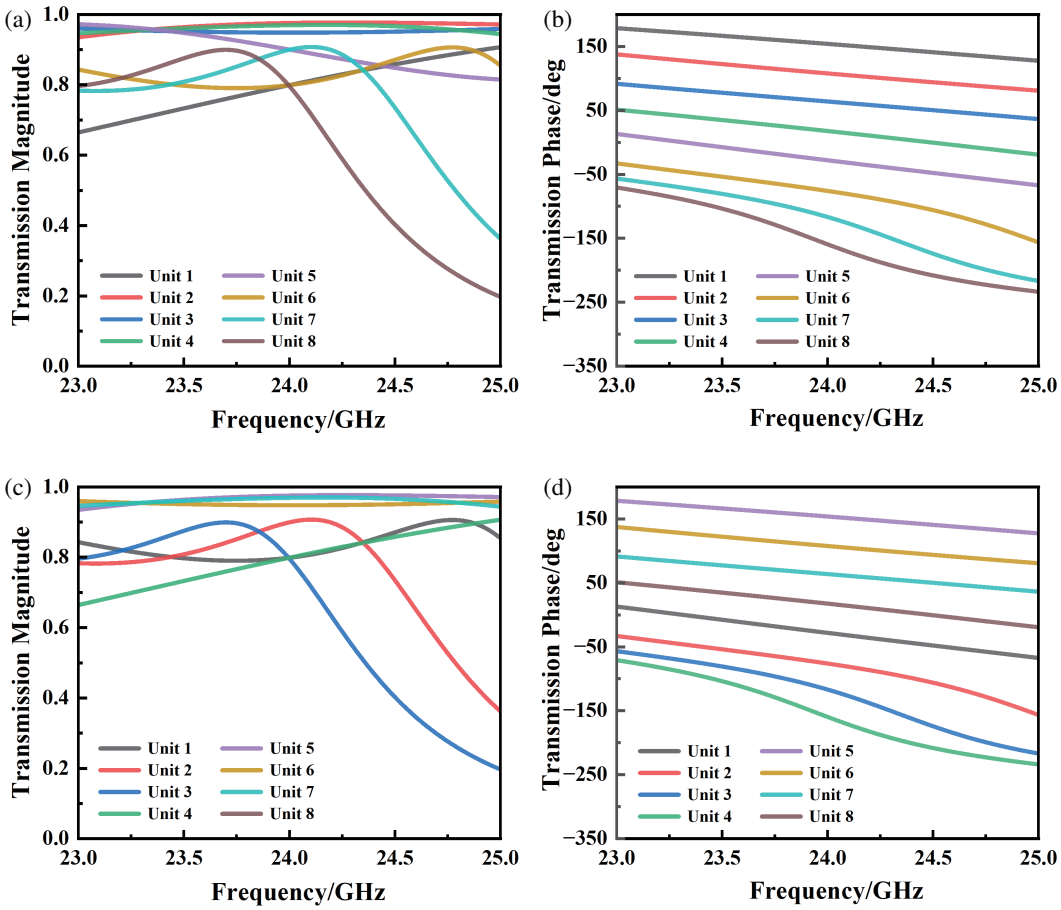

FIGURE 4. Transmission coefficient of 8 selected units. (a) x-polarization transmission amplitude; (b) x-polarization transmission phase; (c) y-polarization transmission amplitude; (d) y-polarization transmission phase.

sion Ratio (PCR):

$$\text{PCR} = \frac{t_{+-}^2}{(t_{+-}^2 + t_{--}^2)} \tag{10}$$

In Equation (10), t_{+-} and t_{--} respectively represent the cross-polarization and co-polarization transmission amplitudes of LHCP waves. According to Equation (10), the PCR of the unit under different parameters θ is calculated, as shown in Fig. 6. It can be observed that near the operating frequency point of 24 GHz, the PCR is close to 100%, indicating that the circular polarization conversion efficiency of the unit is close to 100%. This can be understood as almost all of the electromagnetic waves transmitted through the metasurface are converted into cross-polarization waves.

3. DESIGN OF METASURFACE ARRAY

In order to focus the incident waves in a specified area, it is necessary to construct a metasurface array of certain dimensions based on metasurface units. Design a metasurface array with physical dimensions of 84 mm × 84 mm (20 × 20), with the array plane as the xy plane, the geometric center of the array as the coordinate origin, and the propagation direction of the outgoing waves as the positive z-axis direction. Set the metasurface to vertically incident LHCP waves at 24 GHz, focusing the incident waves at position A (−15 mm, 0 mm, 40 mm); under vertically incident RHCP waves at 24 GHz, focusing the electromagnetic waves at position B (15 mm, 0 mm, 40 mm). The principle of metasurface focusing is shown in Fig. 7.

Use plane waves as the feed source for the metasurface array. When the plane wave passes through the metasurface and reaches the focal point $F(x_f, y_f, z_f)$, the phase $\Delta\phi(x_i, y_j)$ of each unit on the metasurface array should satisfy equation [22]:

$$\Delta\phi(x_i, y_j, 0) = \arg\left\{\exp\left(-j\frac{2\pi}{\lambda}\sqrt{(x_f - x_i)^2 + (y_f - y_j)^2 + z_f^2}\right)\right\} \tag{11}$$

where λ is the wavelength of the incident electromagnetic wave; f_x, f_y, f_z are the coordinates of the focal point; and x_i, y_i are the coordinates of the i-th unit. According to Equation (11), under the conditions of determining the focal point position and unit position, the phase distribution of the metasurface array that can achieve the corresponding focusing effect can be calculated, as shown in Fig. 8(a) and Fig. 8(b).

Under the condition of determining the phase distributions achieving two focusing effects, according to Equations (7) and

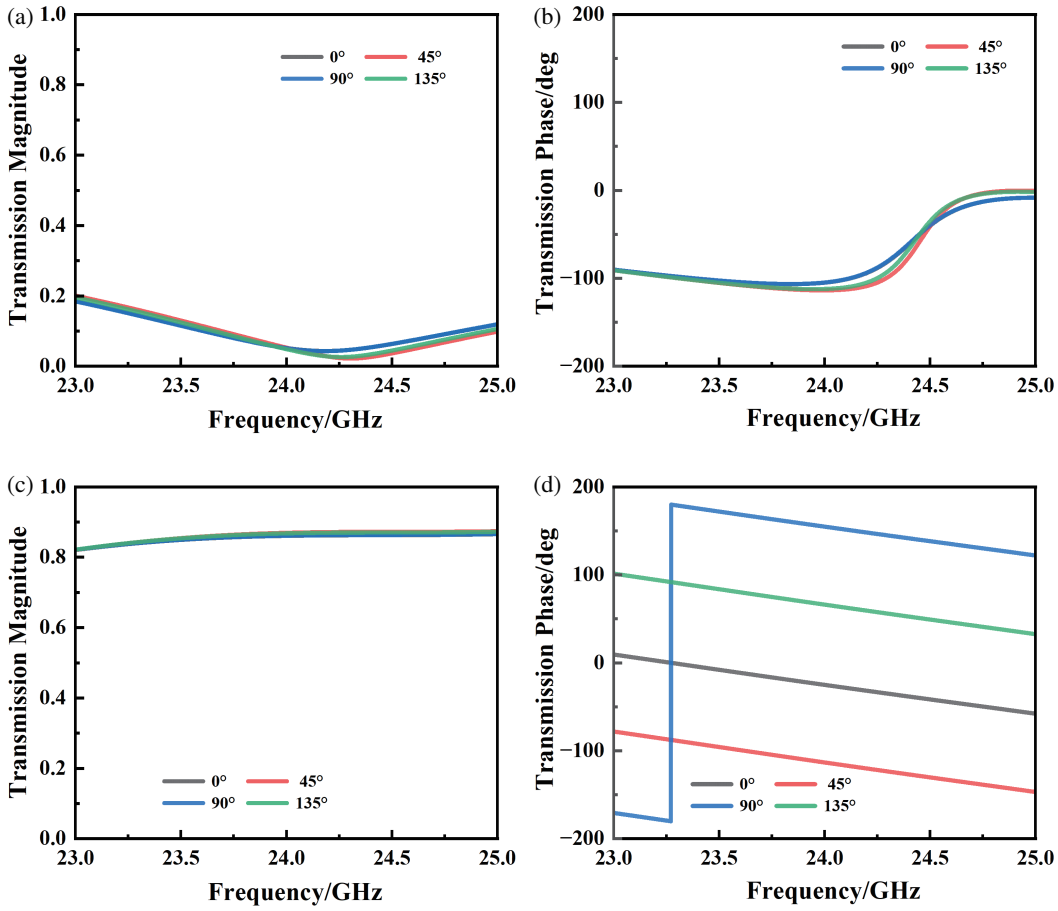

FIGURE 5. The transmission coefficients of units with different θ under LHCP incident. (a) The co-polarized transmission amplitude; (b) The co-polarized transmission phase; (c) The cross-polarized transmission amplitude; (d) The cross-polarized transmission phase.

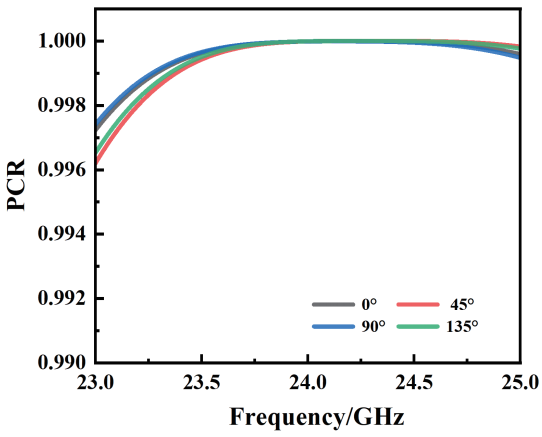

FIGURE 6. Polarization Conversion Ratio of units with different θ.

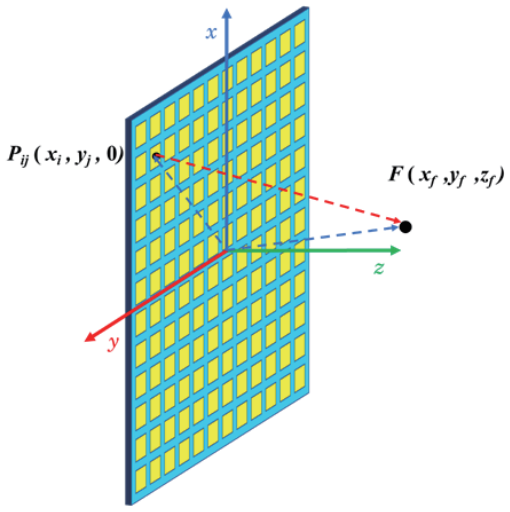

FIGURE 7. The principle of electromagnetic waves focusing by metasurface lens.

(8), the resonant phase distributions $\varphi_x(x_i, y_j)$ and $\varphi_y(x_i, y_j)$ in the x- and y-polarization directions of the metasurface array can be respectively calculated, as shown in Fig. 9(a) and Fig. 9(b). According to Equation (9), the rotation angle $\theta(x_i, y_j)$ of the unit structure can be calculated, as shown in Fig. 9(c).

The phase distribution of the calculated array is discretized with a 45° phase difference based on Fig. 3 and Fig. 4, and the

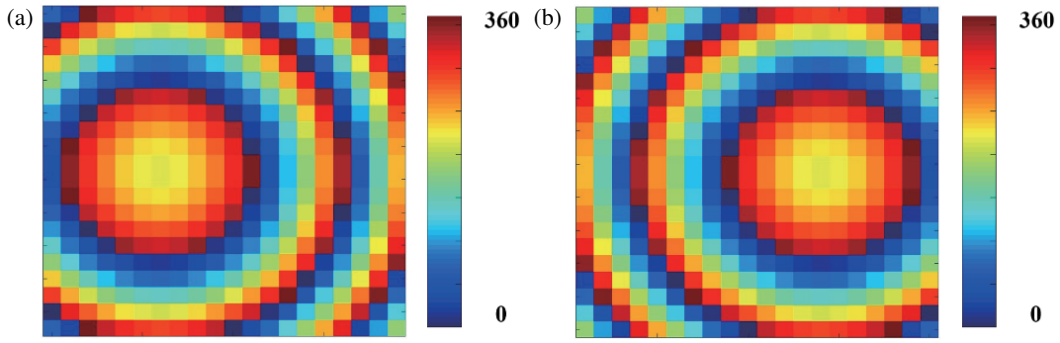

FIGURE 8. Phase distribution of metasurface under circular polarization incident. (a) Left-handed circular polarization; (b) Right-handed circular polarization.

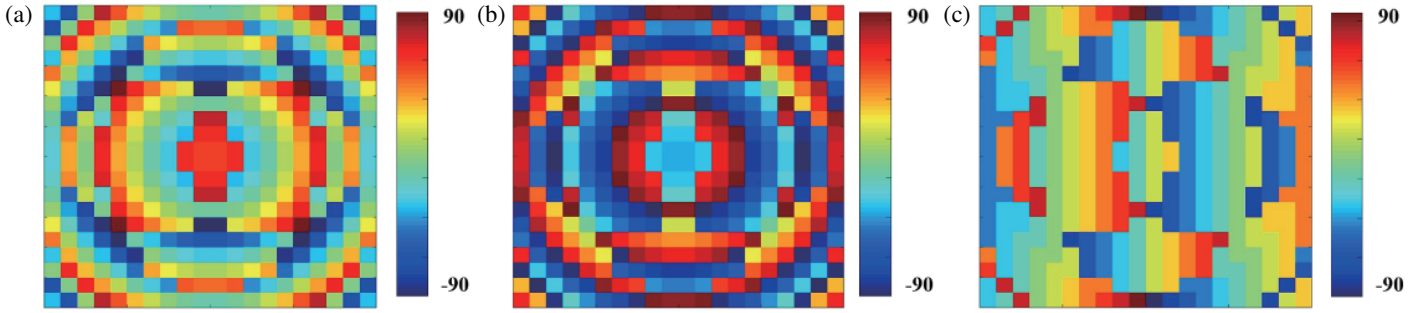

FIGURE 9. Resonance phase distribution and rotation angle. (a) Distribution of x polarization phase; (b) Distribution of y polarization phase; (c) Distribution of unit rotation angles.

specific structure of each unit in the metasurface array can be obtained. Finally, combined with the distribution of unit rotation angles, the entire metasurface array model can be obtained, as shown in Fig. 10.

The designed metasurface array was simulated using CST simulation software, with the front and back of the array selected as the input and output ports, respectively, and plane waves provided by the software were used as the excitation source. LHCP and RHCP plane waves were vertically incident on the metasurface array, resulting in the electric field intensity at the $z = 40$ mm plane as shown in Fig. 11(a) and Fig. 11(b) and the electric field intensity on the xoz plane as shown in Fig. 11(c) and Fig. 11(d).

From Fig. 11, it can be observed that the incident waves achieve a significant focusing effect after passing through the metasurface. Under LHCP and RHCP wave incidence, the electromagnetic waves are converged to different positions, with the maximum electric field intensity located at (-14 mm, 0, 41 mm) and (14 mm, 0, 41 mm), respectively, which are very close to the preset focal point positions. The focusing beam efficiency η is defined as the ratio of the energy at the focus of a metasurface lens to the energy at the plane without the metasurface lens [16, 23]:

$$\eta = P_f / P_0 = \iint Re\left(\vec{E} \times \vec{H}\right) \cdot d\vec{s}_f \Big/ \iint Re\left(\vec{E} \times \vec{H}\right) \cdot d\vec{s}_0 \tag{12}$$

P_f is the focusing power, P the energy irradiated by the horn into the plane when there is no metasurface, s_f the area of the focal spot, and s the area of the plane. Therefore, the focusing efficiencies of the focal points under LHCP and RHCP plane wave incidence can be calculated as 45.9% and 45.6%, respectively. The -3 dB focal widths under LHCP and RHCP wave incidence are shown in Fig. 12. According to Fig. 12(a), the diameter of the focal spot at the $z = 40$ mm plane under LHCP wave incidence is approximately 0.67λ (8.4 mm); similarly, under RHCP wave incidence, the diameter of the focal spot at the $z = 40$ mm plane is approximately 0.7λ (8.8 mm).

The above simulation results demonstrate that the designed circularly polarized multiplexing focusing metasurface can effectively focus LHCP and RHCP waves in the target area, achieving dual-channel single-focus focusing, with high planar resolution and focusing efficiency. The focusing metasurface lens designed in this paper is compared with previous designs, as shown in Table 1. The proposed focusing metasurface has a small thickness and focal size, which enables bifunctional and high-resolution focusing. In addition, it can have a polarization conversion efficiency close to 100%.

4. TESTING AND DISCUSSION

To verify the practical performance of the designed circularly polarized multiplexing focusing metasurface lens, the metasurface lens shown in Fig. 10 was fabricated using planar printing

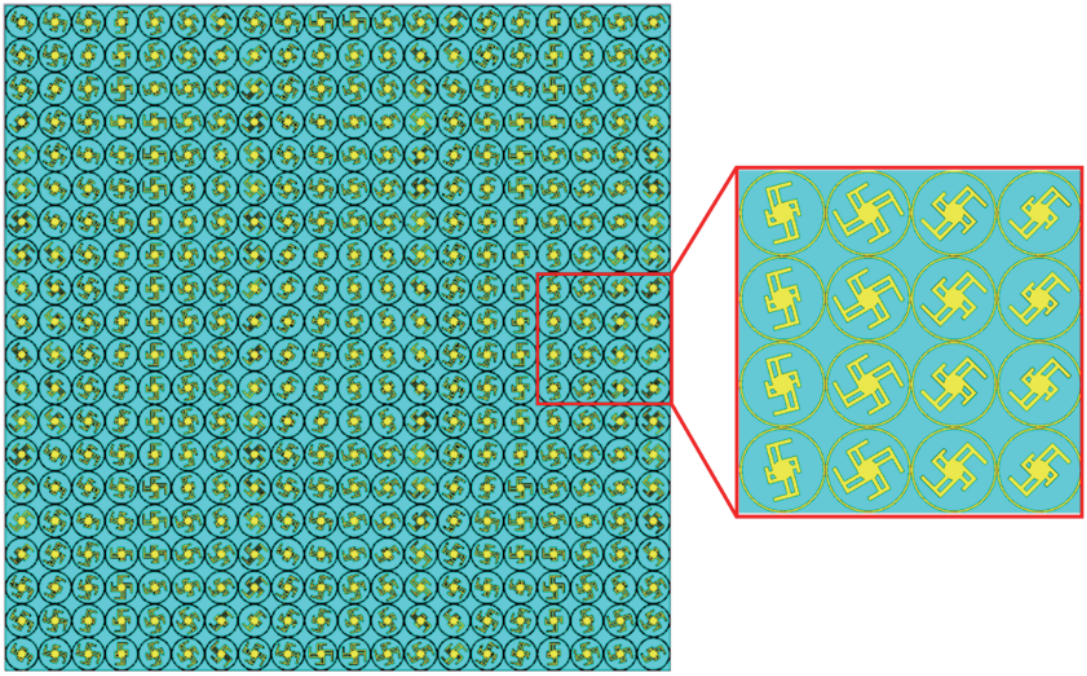

FIGURE 10. Schematic of the metasurface lens structure.

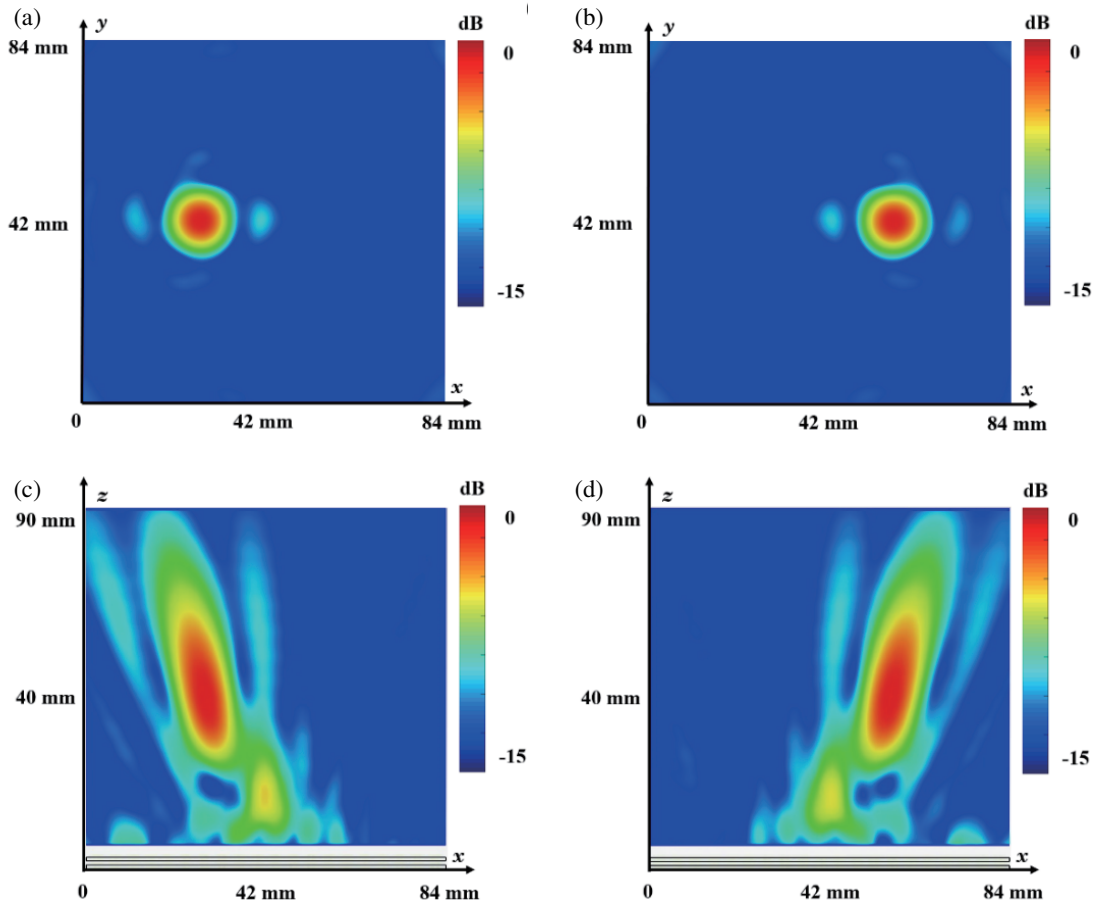

FIGURE 11. Simulation results. (a) Electric field distribution at $z = 40$ mm plane under LHCP incidence; (b) Electric field distribution at $z = 40$ mm plane under RHCP wave incidence; (c) Electric field distribution at $y = 42$ mm plane under LHCP incidence; (d) Electric field distribution at $y = 42$ mm plane under RHCP wave incidence.

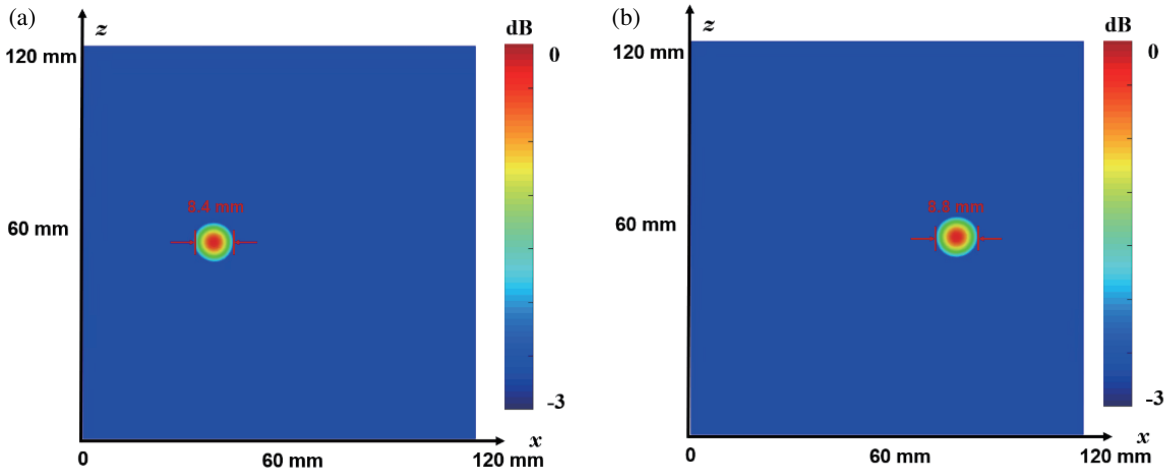

FIGURE 12. The focal width of -3 dB. (a) The Focal spot size in the $z = 40$ mm plane under LHCP wave incidence; (b) The Focal spot size in the $z = 40$ mm plane under RHCP wave incidence.

TABLE 1. Comparison with existing transmissive focused metasurface.

Ref.	Center frequency	polarization	Thickness	PCR	Number of functions	Focus size
[24]	35 GHz	Linear polarization	0.24λ	-	1	1.05λ
[25]	15.5 GHz	Linear polarization	0.21λ	-	2	0.83λ
[26]	10 GHz	Linear polarization	0.08λ	-	1	0.7λ
[15]	35 GHz	Linear polarization	0.18λ	-	1	0.46λ
[17]	15 GHz	Circular polarization	0.075λ	94%	1	0.75λ
This papaer	24 GHz	Circular polarization	0.24λ	99.9%	2	0.67λ

technology. The metasurface consists of 20×20 units, with a planar size of 84×84 mm^2 and a thickness of 3 mm. The metasurface array consists of two identical printed circuit boards (PCBs). The two plates are padded with plastic nuts of 1 mm thickness, so that there is an air layer of 1 mm thickness between the two plates. The fabricated focusing metasurface is shown in Fig. 13(a). The fabricated metasurface lens was placed in a microwave darkroom for measurement, as illustrated in the testing principle in Fig. 13(b).

In the measurement, a circularly polarized horn antenna is used as the feed source, the frequency of the horn antenna is 24 GHz, and the aperture is parallel to the metasurface array, when the distance d of the horn antenna from the metasurface satisfies equation:

$$d > 2D^2/\lambda \tag{13}$$

At this point, the electromagnetic wave radiated by the horn antenna can be approximated as a plane wave at the metasurface. A receiving probe is placed on the other side of the metasurface, and the probe is fixed on a movable mechanical arm, which can translate on a fixed plane to measure the electric field strength distribution on the plane, and the test environment is shown in Fig. 14.

The probe scans within a range of 200×200 mm^2 with a step size of 2 mm. The electric field distribution on the plane is extracted using a vector network analyzer and fitted into a normalized electric field distribution two-dimensional graph. The electric field distribution at $z = 40$ mm under the excitation of LHCP and RHCP waves at 24 GHz for the metasurface sample is illustrated in Fig. 15(a) and Fig. 15(b).

From Fig. 15, it can be observed that the fabricated metasurface sample achieves the single-focus focusing function under the incidence of LHCP and RHCP waves, respectively, and the results are highly similar to the simulation results. To further compare the simulation results with the measured ones, the electric field strength on the line $y = 42$ mm in the $z = 40$ mm plane is extracted under the incidence of LHCP and RHCP

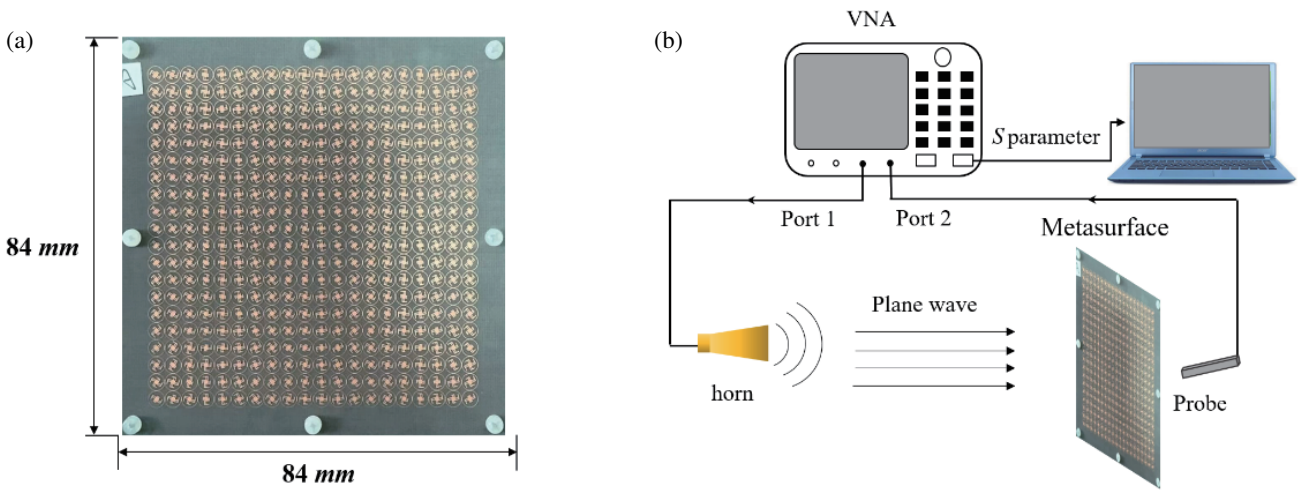

FIGURE 13. Metasurface measurement. (a) Fabricated metasurface. (b) Schematic diagram of the metasurface measurement.

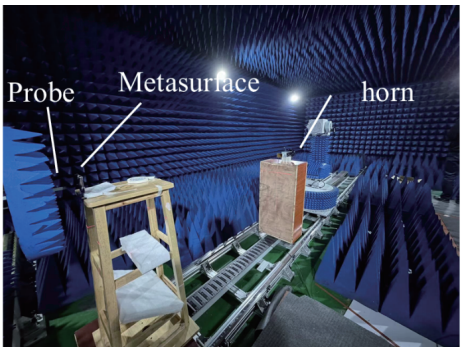

FIGURE 14. Measuring device and environment.

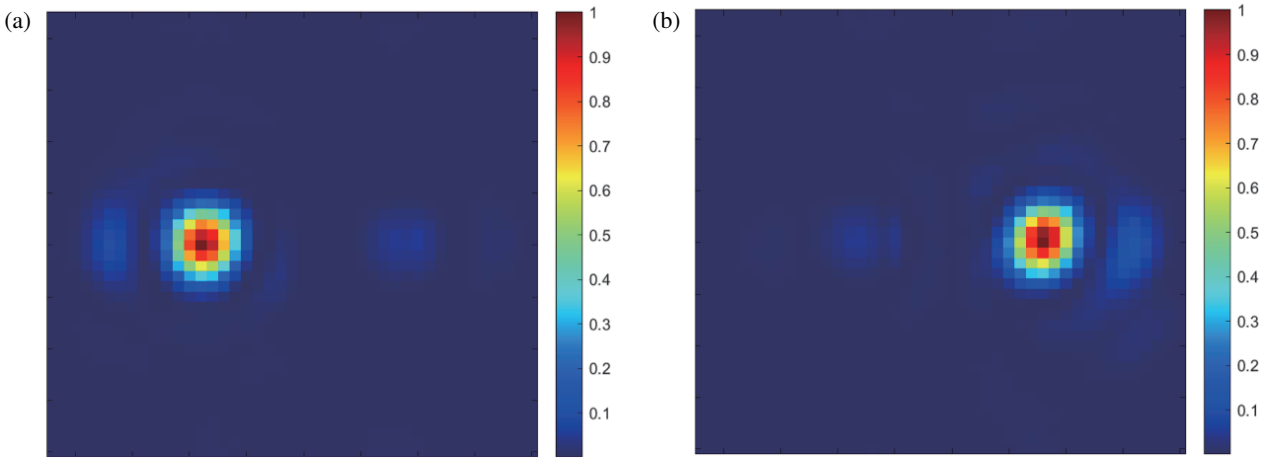

FIGURE 15. Measurement results. (a) Normalized electric field distribution at $z = 40$ mm under 24 GHz LHCP wave incidence; (b) Normalized electric field distribution at $z = 40$ mm under 24 GHz RHCP wave incidence.

waves at 24 GHz, and fitted into a normalized electric field distribution curve, as shown in Fig. 16(a) and Fig. 16(b). The black dashed line in the figure represents the actual test results, while the red solid line represents the simulation results. The simulation results are in good agreement with the actual test results, verifying the effectiveness of the designed circularly polarized reconfigurable focusing metasurface lens.

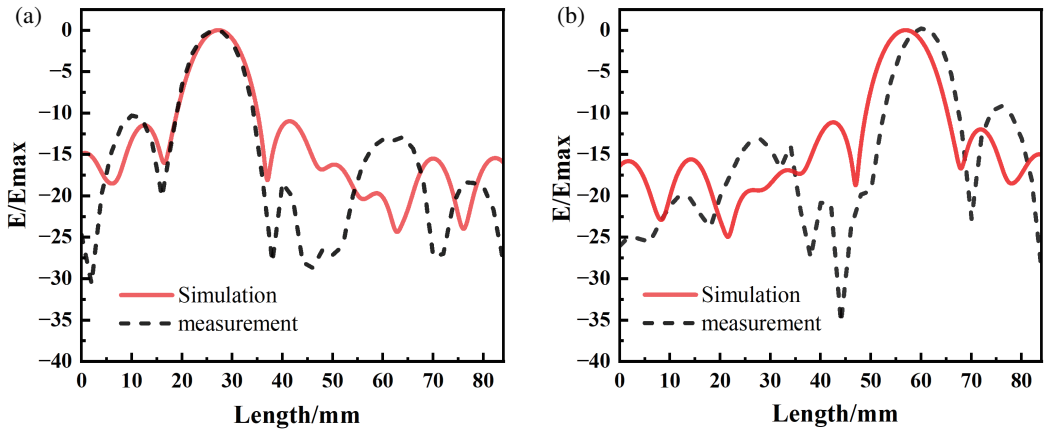

FIGURE 16. Comparison between measured results and simulation results. (a) The normalized electric field distribution on the line $y = 42$ mm under LHCP wave incident at 24 GHz; (b) Normalized electric field distribution on line $y = 42$ mm at the incidence of RHCP wave at 24 GHz.

5. CONCLUSION

In this paper, a two-layer circularly polarized multiplexed focusing metasurface lens is designed and processed, which can focus the circularly polarized incident wave at the target position while achieving a highly efficient polarization conversion function. The decoupling of the LHCP and RHCP phase distributions is achieved by the method of joint modulation of resonance and Pancharatnam-Berry phase, which enables the metasurface array to achieve different focusing effects under the incidence of LHCP and RHCP waves. The polarization conversion ratio is close to 100%. Simulated and experimental results show that the metasurface lens achieves two different focusing effects under LHCP and RHCP irradiation with good focusing effects; the focusing efficiencies are 45.6% and 45.9%, respectively; the -3 dB focal spot size sizes are 0.7λ (8.8 mm) and 0.67λ (8.4 mm), respectively; and the metasurface lens has a polarization. The ultra-surface lens is characterized by high polarization conversion efficiency, high spatial resolution, multifunctionality, and small size, which has potential applications in K-band satellite communications, wireless power transmission, and 24 GHz vehicle-mounted millimeter-wave radar.

ACKNOWLEDGEMENT

This work was supported by Chongqing Natural Science Foundation General Program (No. CSTB2022NSCQ-MSX0960).

Data Availability

The authors confirm that the data supporting the findings of this study are available within the article.

Disclosures

The authors declare no conflicts of interest.

REFERENCES

[1] Toh, B. Y., R. Cahill, and V. F. Fusco, "Understanding and measuring circular polarization," *IEEE Transactions on Education*, Vol. 46, No. 3, 313–318, 2003.

[2] Wu, Z., L. Li, Y. Li, and X. Chen, "Metasurface superstrate antenna with wideband circular polarization for satellite communication application," *IEEE Antennas and Wireless Propagation Letters*, Vol. 15, 374–377, 2015.

[3] Wang, Y., H. Shi, J. Chen, J. Yi, L. Dong, A. Zhang, and H. Liu, "Digital polarization programmable metasurface for continuous polarization angle rotation and radar applications," *Frontiers in Materials*, Vol. 9, 931868, 2022.

[4] Han, T., K. Wen, Z. Xie, and X. Yue, "An ultra-thin wideband reflection reduction metasurface based on polarization conversion," *Progress In Electromagnetics Research*, Vol. 173, 1–8, 2022.

[5] Peng, S. S., L. Wu, X. H. Ying, and Z. C. Xu, "A receiver in a millimeter wave radiometer for atmosphere remote sensing," *Journal of Infrared, Millimeter, and Terahertz Waves*, Vol. 30, 259–269, 2009.

[6] Li, P., M. Lewin, A. V. Kretinin, J. D. Caldwell, K. S. Novoselov, T. Taniguchi, K. Watanabe, F. Gaussmann, and T. Taubner, "Hyperbolic phonon-polaritons in boron nitride for near-field optical imaging and focusing," *Nature Communications*, Vol. 6, No. 1, 1–9, 2015.

[7] Nanzer, J. A., A. Wichman, J. Klamkin, *et al.*, "Millimeter-wave photonics for communications and phased arrays," *Fiber and Integrated Optics*, Vol. 34, No. 4, 159–174, 2015.

[8] Buffi, A., A. A. Serra, P. Nepa, H. T. Chou, and G. Manara, "A focused planar microstrip array for 2.4 GHz RFID readers," *IEEE Transactions on Antennas and Propagation*, Vol. 58, No. 5, 1536–1544, 2010.

[9] Zhao, J., H. Ye, K. Huang, Z. N. Chen, B. Li, and C.-W. Qiu, "Manipulation of acoustic focusing with an active and configurable planar metasurface transducer," *Scientific Reports*, Vol. 4, No. 1, 6257, 2014.

[10] Grbic, A. and R. Merlin, "Near-field focusing plates and their design," *IEEE Transactions on Antennas and Propagation*, Vol. 56, No. 10, 3159–3165, 2008.

[11] Ratni, B., A. De Lustrac, G.-P. Piau, and S. N. Burokur, "Modeling and design of metasurfaces for beam scanning," *Applied Physics A*, Vol. 123, 1–7, 2017.

[12] Bai, X., "High-efficiency transmissive metasurface for dual-polarized dual-mode OAM generation," *Results in Physics*, Vol. 18, 103334, 2020.

[13] Lin, D., A. L. Holsteen, E. Maguid, P. Fan, P. G. Kik, E. Hasman, and M. L. Brongersma, "Polarization-independent metasurface lens employing the Pancharatnam-Berry phase," *Optics Express*, Vol. 26, No. 19, 24 835–24 842, 2018.

[14] Li, J.-s. and J.-q. Yao, "Manipulation of terahertz wave using coding Pancharatnam–Berry phase metasurface," *IEEE Photonics Journal*, Vol. 10, No. 5, 1–12, 2018.

[15] Chu, H., J. Qi, S. Xiao, and J. Qiu, "A thin wideband high-spatial-resolution focusing metasurface for near-field passive millimeter-wave imaging," *Applied Physics Letters*, Vol. 112, No. 17, 2018.

[16] Zhang, P., L. Li, X. Zhang, H. Liu, and Y. Shi, "Design, measurement and analysis of near-field focusing reflective metasurface for dual-polarization and multi-focus wireless power transfer," *IEEE Access*, Vol. 7, 110 387–110 399, 2019.

[17] Guo, W.-L., G.-M. Wang, H.-P. Li, and H.-S. Hou, "Utra-thin single-layered high-efficiency focusing metasurface lens," *Acta Physica Sinica*, Vol. 65, No. 7, 2016.

[18] Balthasar Mueller, J. P., N. A. Rubin, R. C. Devlin, B. Groever, and F. Capasso, "Metasurface polarization optics: Independent phase control of arbitrary orthogonal states of polarization," *Physical Review Letters*, Vol. 118, No. 11, 113901, 2017.

[19] Liu, M., P. Huo, W. Zhu, C. Zhang, S. Zhang, M. Song, S. Zhang, Q. Zhou, L. Chen, H. J. Lezec, A. Agrawal, Y. Lu, and T. Xu, "Broadband generation of perfect poincaré beams via dielectric spin-multiplexed metasurface," *Nature Communications*, Vol. 12, No. 1, 2230, 2021.

[20] Berry, M. V., "Quantal phase factors accompanying adiabatic changes," *Proceedings of the Royal Society of London. A. Mathematical and Physical Sciences*, Vol. 392, No. 1802, 45–57, 1984.

[21] Hao, H., Y. Tang, S. Zheng, X. Ran, and W. Ruan, "Design of circular polarization multiplexing beam splitter based on transmission metasurface," *Progress In Electromagnetics Research M*, Vol. 109, 125–136, 2022.

[22] Hao, H., Z. Cai, P. Tang, and B. Li, "Design of a polarization-multiplexed, high-resolution, near-field focusing metasurface lens," *Applied Optics*, Vol. 63, No. 10, A78–A85, 2024.

[23] Zhang, K., Y. Yuan, X. Ding, B. Ratni, S. N. Burokur, and Q. Wu, "High-efficiency metalenses with switchable functionalities in microwave region," *ACS Applied Materials & Interfaces*, Vol. 11, No. 31, 28 423–28 430, 2019.

[24] Li, J., Z. Wang, Y. Ma, X. Ran, and H. Hao, "Design of high-resolution near-field focusing metasurface lens," *Journal of Electromagnetic Waves and Applications*, Vol. 35, No. 16, 2115–2124, 2021.

[25] Huang, H. and J. Zhang, "Multifunctional near field focusing transmission metasurface based on polarization sensitivity," *Microwave and Optical Technology Letters*, Vol. 63, No. 7, 1868–1874, 2021.

[26] Liu, Y.-Q., Z. Ren, Y. Shu, L. Wu, J. Sun, H. Cai, X. Zhang, L. Lu, K. Qi, L. Li, Y. Che, and H. Yin, "Broadband, large-numerical-aperture and high-efficiency microwave metalens by using a double-layer transmissive metasurface," *Applied Physics Express*, Vol. 15, No. 1, 014003, 2022.